

Nanoscale

Accepted Manuscript



This is an *Accepted Manuscript*, which has been through the Royal Society of Chemistry peer review process and has been accepted for publication.

Accepted Manuscripts are published online shortly after acceptance, before technical editing, formatting and proof reading. Using this free service, authors can make their results available to the community, in citable form, before we publish the edited article. We will replace this *Accepted Manuscript* with the edited and formatted *Advance Article* as soon as it is available.

You can find more information about *Accepted Manuscripts* in the [Information for Authors](#).

Please note that technical editing may introduce minor changes to the text and/or graphics, which may alter content. The journal's standard [Terms & Conditions](#) and the [Ethical guidelines](#) still apply. In no event shall the Royal Society of Chemistry be held responsible for any errors or omissions in this *Accepted Manuscript* or any consequences arising from the use of any information it contains.

Cite this: DOI: 10.1039/c0xx00000x

www.rsc.org/ xxxxxx

PAPER

In situ assembly of well-dispersed Ni nanoparticles on silica nanotubes and excellent catalytic activity in 4-nitrophenol reduction

Shenghuan Zhang,^a Shili Gai,^a Fei He,^a Shujiang Ding^{*b}, Lei Li^a and Piaoping Yang^{*a}

Received (in XXX, XXX) Xth XXXXXXXXX 20XX, Accepted Xth XXXXXXXXX 20XX

DOI: 10.1039/b000000x

The easy aggregation nature of the ferromagnetic nanoparticles (NPs) prepared by the conventional routes usually leads to large particle size and low loading amount, which greatly limits their application in reduction of 4-nitrophenol (4-NP). Herein we developed a novel *in situ* thermal decomposition and reduction strategy to prepare Ni nanoparticles/silica nanotubes (Ni/SNTs), which can markedly prevent the aggregation and growth of Ni NPs, resulting in the ultra small particle size (about 6 nm), good dispersion and especially high loading amount of Ni NPs. It is found that Ni/SNTs which preserve high specific surface area (416 m²/g) exhibit ultra high catalytic activity in the 4-NP reduction (complete reduction of 4-NP within only 60 s at room temperature), which is superior to most noble metal (Au, Pt, and Pd) supported catalysts. Ni/SNTs still show high activity even after re-use for several cycles, suggesting the good stability. In particular, the magnetic property of Ni/SNTs makes it easy to recycle for reuse.

1. Introduction

Inorganic nanotubes have been attracted considerable interest since the discovery of carbon nanotubes (CNTs).¹ One-dimensional (1-D) nanotubes have unique chemical and physical properties, such as nano-sized thick wall and high specific interface area, which make them highly potential in drug delivery,² photoluminescence,³ gas sensing,⁴ and catalysts.⁵⁻⁷ Besides CNTs, various other inorganic nanotubes have been extensively reported, including silica,⁸ metal oxides⁹ and metals.^{10,11} However, ferromagnetic nanotubes have rarely been reported because of the tendency of ferromagnetic metals to oxidize despite their technological importance. Ferromagnetic nanotubes are usually multifunctional materials which combine the unique properties of the nanotubes, such as high specific interface area, and the magnetic property of metal particles together.¹² Therefore, these magnetic nanostructures have stimulated extensive research efforts in recent years especially in catalysts.¹³ Among various synthetic methods, electrodeposition method and template method are most popular. Ferromagnetic Fe, Co and metal oxide nanotubes have been reported using tobacco mosaic virus, silica nanotubes (SNTs) and DNA as templates.¹⁴⁻¹⁶ But there is very little report on fabricating magnetic Ni nanoparticles (Ni NPs) supported nanotubes. It is noted that the physiochemical properties of Ni NPs are superior to the bulk materials, which are more efficient in catalytic activity due to their large surface area-to-volume ratio. However, it is well known that smaller nanoparticles usually tend to aggregate, which greatly limit their application.¹⁷ Therefore, it is highly promising to develop new approaches to prepare smaller Ni NPs with high dispersion.

4-aminophenol (4-AP) is a vital intermediate for the manufacture of analgesic and antipyretic drugs,¹⁸ while 4-nitrophenol (4-NP) is a common organic pollution in the industrial and agricultural waste water.¹⁹ An efficient and environmentally friendly conversion route is the direct reduction of 4-NP to 4-AP in the presence of NaBH₄. To make the route come true, various noble metals including Au, Ag, Pt, Au-Ag and Au-Pt nanocatalysts have been widely employed due to their efficient catalytic activities.²⁰⁻²⁴ However, smaller nanoparticles tend to be easily aggregated due to their large surface area-to-volume ratio and are hard to be removed from the reaction media, and especially the high cost of noble metal limits their applications. Thus, in order to reduce the expense of noble metal catalysts, transition metal catalysts are becoming more and more popular due to their markedly lower cost.²⁵⁻²⁷ As far as we know, the reduction time of 4-NP to 4-AP over noble metal catalysts is at least 120 s, while the reduction time for transition metal catalysts is far long compared with noble metal catalysts.^{25,28-32} Therefore, a great challenge is to improve the catalytic activities of the transition metal supported nanotubes catalysts.

In this study, we for the first time developed a novel method to synthesize Ni NPs supported silica nanotubes (Ni/SNTs) *via* a two-step method. This unique *in situ* thermal decomposition and reduction method from nickel silicate (NiSNTs) precursor can markedly prevent the aggregation and growth of Ni NPs, resulting in ultra small particle size, good dispersion and high loading amount of Ni NPs. To the best of our knowledge, this is the first time silicate nanotubes precursor has been utilized for the production of high dispersed Ni NPs catalysts. The catalytic performance and the stability of Ni/SNTs in 4-NP reduction have

also been systematically investigated.

2. Experimental section

2.1. Synthesis

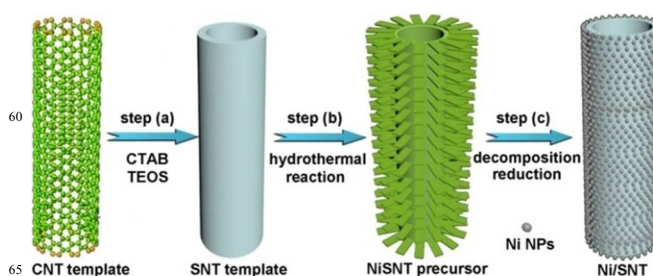
Synthesis of silica nanotubes. Silica nanotubes were synthesized by CNT templates.³³ In a typical procedure, 150 mg of CNT was added to a solution of 150 mL H₂O, 100 mL ethanol and 0.62 g CTAB at room temperature. After sonication for 6 h, 300 μ L NaOH (1 M) was added to the above solution under stirring. Then 1.2 mL TEOS was added drop-wise and stirring for 12 h. The black solid products were then collected, purified and dried overnight. The white silica nanotubes were obtained by calcined at 550 $^{\circ}$ C for 5 h in air flow.

Synthesis of NiSNTs. At room temperature, a certain amount of nickel chloride (ranging from 0.1 mmol to 0.75 mmol, analytical grade) and ammonia chloride (10 mmol, analytical grade) were dissolved in deionizer water (30 mL), and ammonia solution (1 mL, 28%) was added under stirring, the color of the solution was transformed from light green to deep blue immediately. 40 mg as-prepared silica nanotubes was dispersed homogeneously in 10 mL deionized water. The above two solution were mixed homogeneously and then transferred into a Teflon autoclave (50 mL) and heated to a temperature of 100 $^{\circ}$ C for 16 h. After cooling to room temperature, a green precipitate was collected by centrifugation and washed with deionized water and ethanol three times. The nickel silicate nanotubes were finally obtained after dried at 60 $^{\circ}$ C for 12 h.

Synthesis of Ni/SNTs. 40 mg NiSNTs was placed in a ceramic boat in the middle of the horizontal tube furnace. The Ni/SNTs were obtained by calcinating nickel silicate under H₂/N₂ mixture (typically 5% H₂) at 800 $^{\circ}$ C for 8 h. Black power was collected in the ceramic boat at room temperature.

Catalytic reaction. The reduction of 4-NP by NaBH₄ was chosen as a model reaction for investigating the catalytic performance of the multifunctional Ni/SNTs. Typically, 1.85 mL ultrapure water, 100 μ L 4-NP solution (5 mM) and 1.0 mL freshly prepared NaBH₄ aqueous solution (0.2 M) were added into a standard quartz curette respectively. The solution turned from light yellow to bright yellow immediately after NaBH₄ aqueous was added. Subsequently, 4 mg Ni/SNTs were added to start the reaction. The color of the mixture gradually vanished, indicating the reduction of the 4-NP. Changes in the concentration of 4-NP were monitored by the UV-vis absorption which were recorded in the scanning range of 250-500 nm at room temperature. Different amount of Ni/SNTs were also used as the catalysts adding to the reaction solution for the reduction of 4-NP.

Characterization. X-ray diffraction (XRD) measurement was examined on a RigakuD/max-TTR-III diffractometer using monochromatic Cu K α radiation ($\lambda = 0.15405$ nm). The morphologies of the samples were inspected on a scanning electron microscope (SEM, Hitachi S-4800). Transmission electron microscopy (TEM) and high-resolution transmission electron microscopy (HRTEM) micrographs were performed on a FEI Tecnai G² S-Twin transmission electron microscope with a field emission gun operating at 200 kV. Images were acquired digitally on a Gatan multiple CCD camera. N₂



Scheme 1 Schematic illustration of the synthetic procedure for Ni/SNTs.

adsorption/desorption were measured at 77 K using a Micromeritics TriStar 3020 instrument. The specific surface area was calculated by the Brunauer-Emmett-Teller (BET) method, and pore size distribution was calculated from the desorption branch of the isotherm. Inductively coupled plasma (ICP) analysis (Thermo iCAP 6000 ICPOES) were used to measure the elemental compositions for the samples. Magnetization measurements were performed on a MPM5-XL-5 superconducting quantum interference device (SQUID) magnetometer at 300 K. The absorbance of 4-NP was obtained on a TU-1901 UV/vis spectrophotometer.

Result and discussion

Scheme 1 depicts the synthetic strategy of well dispersed Ni NPs on silica nanotubes (Ni/SNTs). The silica nanotubes templates were first synthesized *via* dual templates route by selecting carbon nanotubes and cetyltrimethyl ammonium bromide (CTAB) as the hard and soft template, respectively. Then lamellar structured NiSNTs precursors were obtained by hydrothermal reaction in alkaline condition at high temperature, which involves the process of breaking silica chains of silica nanotubes to form silicate-ion groups and then reacting with nickel ions to form nickel silicate NTs in the solution.³¹ Finally, Ni/SNTs were obtained through an *in situ* decomposition and reduction procedure in hydrogen atmosphere at high temperature.

In Fig. 1, it is found that SNTs have hollow structure with narrow diameter distribution and open ends (Fig. 1a, b). The size distribution histogram displays inset Fig. 1a reveals that the inner diameter and outer diameter mainly centred at 20 nm and

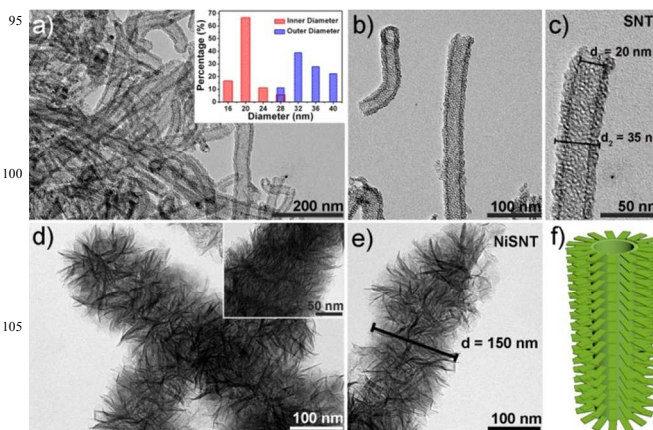


Fig. 1 a) TEM image, b) magnified TEM image and c) a single nanotube of silica nanotube; d) TEM image, e) a single nanotube and f) morphology sketch of NiSNTs. Inset in panel a is the size distribution histogram of the inner diameter and outer diameter.

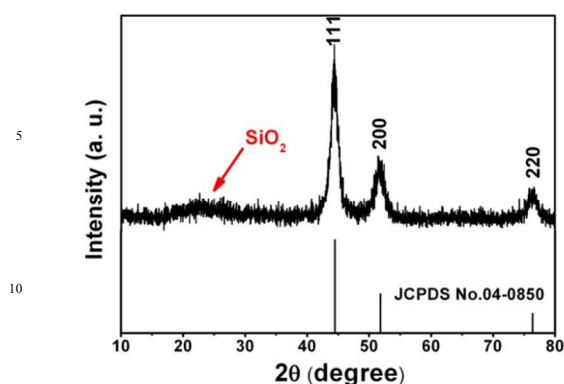


Fig. 2 XRD pattern of Ni/SNTs and the standard data of cubic phased Ni.

32 nm respectively, suggesting that the wall thickness is about 6 nm. And the wall thickness of a single SNTs is calculated to be about 7.5 nm (Fig. 1c). Fig. S1 displays XRD pattern and TEM image of SNTs after calcination at 800 °C for 8 hours. The amorphous peak centred around 22° and the good tube structure of SNTs suggests that the as-synthesized SNTs templates exhibit high stability under high temperature which indicates it is very suitable for catalytic reaction. The porous structure of SNTs wall is very suitable to fabricate silicate materials and the micropores make nickel ions and other ions in water solution easy to diffuse into SNTs and react with silicate ions to form nickel silicates *in situ*.³² The XRD diffractions (Fig. S2) of the as-prepared precursor can be indexed to nickel silicate hydrates. The EDS analysis shows three Ni, Si and O elements in the sample (Fig. S3). From the TEM image of the NiSNTs precursor (Fig. 1d,e), we can see that the surface of NiSNTs are much rougher than that of SNTs, which consists of uniform petal-like units assembled into a tubular shaped structure. The inset in Fig. 3d shows the petal-like units are very thin nanosheets. In Fig. 1e, the diameter of NiSNTs is calculated to be about 150 nm, which is almost four times larger than that of the outer diameter of silica nanotubes. This is because in the *in situ* reaction process, after the nickel ions react with the silicate ions on the surface, the inner silica chains will dissolve and move to the surface and go on reaction.³¹ It is noted that the hollow structure of NiSNTs is not obvious which may be due to the relatively thick wall that the electron beam cannot penetrate. The morphology sketch (Fig. 1f) shows the profile of the tubular structure assembled by petal-like units.

In the XRD pattern of Ni/SNTs (Fig. 2), all the sharp diffractions can be well indexed to cubic-phased Ni (JCPDS No. 04–0850). And no other phases can be detected except for a low broad band at $2\theta = 22^\circ$ assigned to amorphous silica, indicating that lamellate nickel silicate have been completely converted to metal Ni and amorphous silica. The results suggest that Ni NPs are both inside and outside of SNTs supports for the *in situ* calcination progress. The average crystallite size of Ni NPs calculated by the Scherrer-equation is 6.8 nm, which is in agreement with the following TEM result (Fig. 3b). From the TEM image (Fig. 3a), we can see that the nanotubes are composed of numerous nanoparticles, which are much different from the silicates precursor assembled by thin flakes. The sample still keeps the 1-D structure with narrow size distribution. In the magnified TEM image of a single Ni/SNT (Fig. 3b), the diameter of a nanotube is calculated to be 100 nm, which is much smaller

than the precursor (150 nm) while much larger than the silica nanotubes template. The change of the diameters during the reaction can be explained as follows. The decomposition of the loose lamellate nickel silicate into dense metal Ni layer leads to the decrease of diameter. The SEM images (Fig. S4) of a single SNTs, NiSNTs and Ni/SNTs match well with the corresponding TEM images in Fig. 1 and Fig. 3. The inset of Fig. 3b is the selected area electron diffraction (SAED) pattern of Ni/SNTs. The presence of the concentric rings further confirms the formation of the cubic-phased Ni. In the HRTEM image (Fig. 3c), the spherical Ni NPs with the particle size of about 6 nm can be easily observed. And Fig. S5 displays the enlarge HRTEM image of Ni/SNTs. The distance of the adjacent lattice fringes (marked by the arrows) is determined to be about 0.203 nm, corresponding well to the d_{111} spacing of cubic Ni (JCPDS No. 04–0850). Inset of Fig. 3c is the corresponding fast Fourier transform (FFT) pattern. The three pairs of diffraction spots reveals the crystalline nature of the sample and any pairs of them can be calculated to the (111) planes of cubic Ni. The size distribution histogram of the Ni NPs reveals that Ni NPs are uniform in diameter with a relatively narrow distribution centered at 6 nm to 7 nm. In the EDS (Fig. 3e), Si, O, Ni elements can be found, and C is from the carbon conductive tape. It is clear that the high Ni loading amount has been achieved. Additionally, we can see that Ni, Si and O are uniformly dispersed along the silica nanotubes from the TEM mapping of Ni/SNTs. The high dispersion of Ni atoms should be due to the unique thermal decomposition and subsequent reduction process.

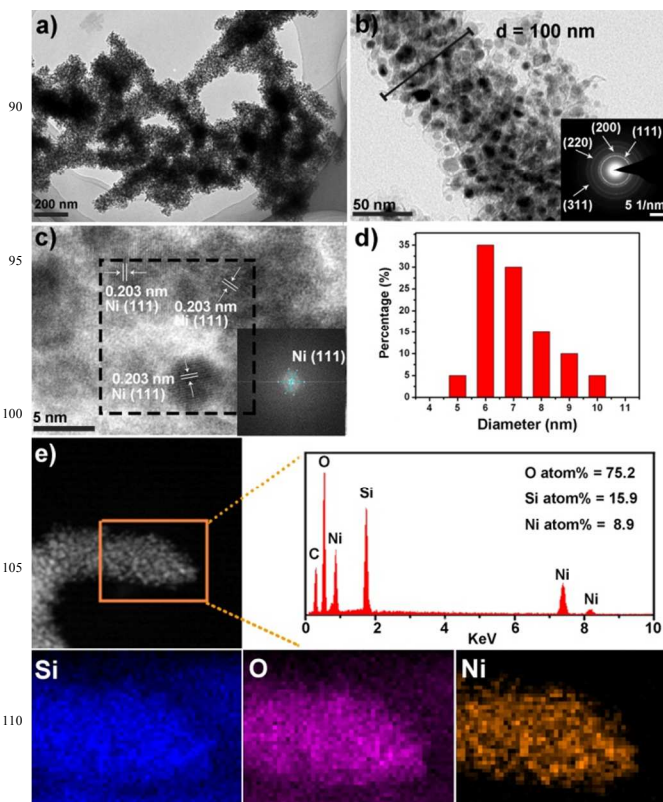


Fig. 3 a) Low-, b) high-magnification TEM images (inset is the SAED pattern), c) HRTEM image (inset is corresponding FFT pattern), d) size distribution histogram of the Ni NPs, and e) EDS and mapping of Ni/SNTs.

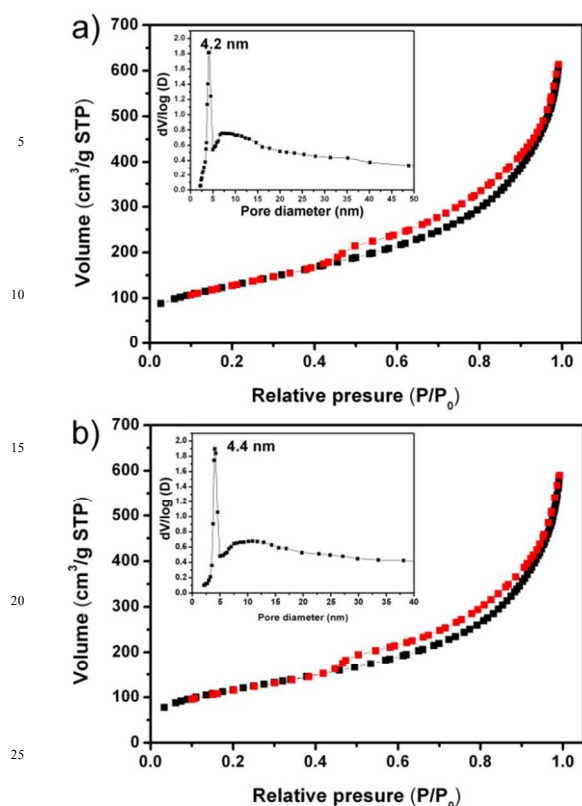


Fig. 4 N_2 adsorption/desorption isotherms of a) NiSNTs, b) Ni/SNTs and their corresponding pore size distributions (insets).

Table 1 BET surface area, average pore diameter and total volume of CNTs, SNTs, NiSNTs and Ni/SNTs.

Samples	S_{BET} (m^2/g)	D (nm)	V_P (cm^3/g)
CNTs	112	28.85	0.57
SNTs	896	6.04	1.41
NiSNTs	458	8.93	0.93
Ni/SNTs	416	9.42	0.89

* S_{BET} , the BET specific surface area calculated in the relative pressures range from 0.05 to 0.2; D , the average diameter of mesopores calculated by the BJH method; V_P , the total pore volume calculated at the relative pressure of about 0.95.

Fig. 4 shows the N_2 adsorption/desorption isotherms and pore size distributions (inset) of NiSNTs and Ni/SNTs, respectively. Each isotherm can be classified to a type-IV isotherm with a small hysteresis loop, indicating the presence of textural mesopores. The textural parameters of CNTs, SNTs, NiSNTs and Ni/SNTs are summarized in Table 1. It is found that both the specific surface area and pore volume of SNTs are markedly enhanced compared with CNTs, which may be attributed to the introduced soft template (CTAB). The respective BET surface of NiSNTs and Ni/SNTs is calculated to be $458 m^2/g$ and $416 m^2/g$, showing large BET surface areas and narrow pore size distribution (insets in Fig. 4), suggesting the potential application of this product as catalysts support.

Fig. 5 shows the magnetization curve of Ni/SNTs at room temperature. The saturation magnetization value is $22.6 emu/g$. It is well known that magnetic NPs smaller than 20 nm are usually superparamagnetic at room temperature due to the higher thermal fluctuation energy compared with energy.^{35,36} In Fig. 5, nearly no

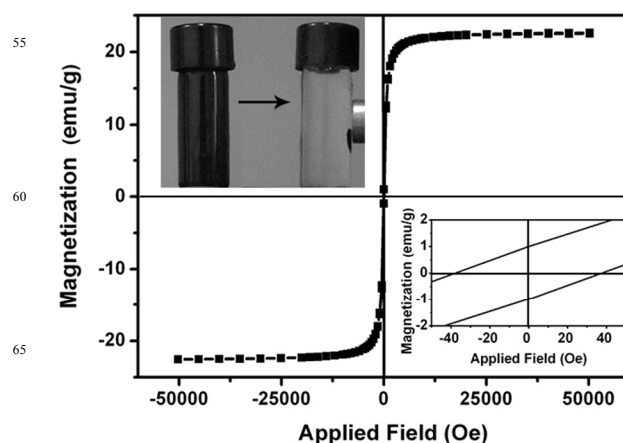


Fig. 5 Magnetization curves of Ni/SNTs at room temperature. The inset is the photograph for the magnetic separation (up left) and the enlargement near origin (low right).

coercivity or remanence can be found and the coercivity is 38 Oe from the enlarged magnetization curve (inset in Fig. 5), revealing the sample is very close to the superparamagnetic state. The photograph of the magnetic separation (inset) demonstrates the easy manipulation of Ni/SNTs by an external magnetic field, which makes it possible to be recycled for reuse.

The mechanism of this unique *in situ* calcination and reduction method has been put forward by tracing the XRD patterns of the

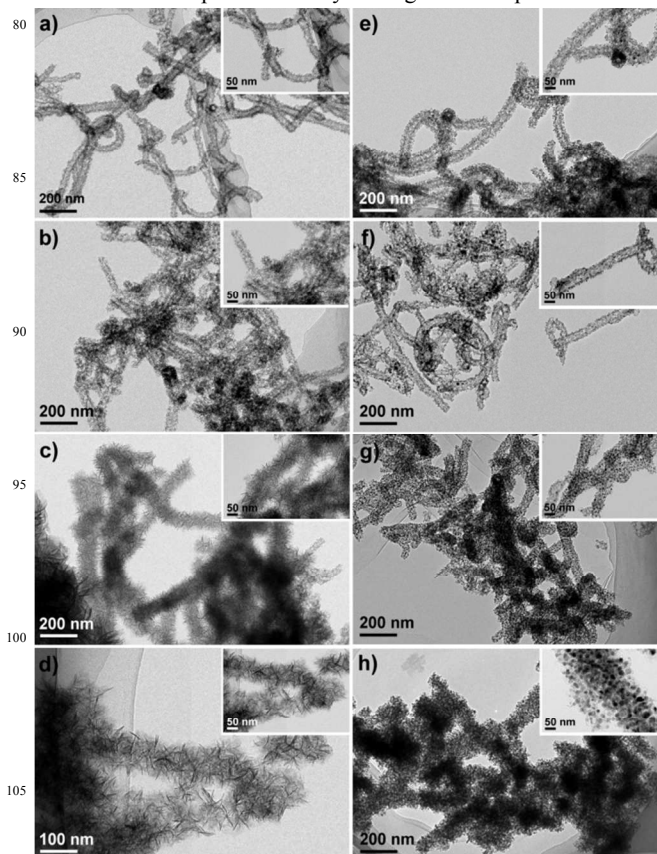


Fig. 6 TEM images of NiSNTs synthesized by adding 0.1 mmol, 0.25 mmol, 0.5 mmol and 0.75 mmol $NiCl_2$ for hydrothermal reaction (a-d) and their corresponding TEM images of Ni/SNTs (e-h) after calcination at $800^\circ C$.

samples after calcination and reduction with different reaction time (Fig. S6) and calcination in the air (Fig. S7). Except for the peaks of cubic Ni and SiO₂ in Fig. S6, weak peaks centred at around 35° and 62° are found, which can be indexed to nickel silicate hydrate when the reaction time is 0.5 h, 2 h, and 4 h. Fig. S7 displays the XRD pattern of sample calcined in the air at 800 °C for 8 hours, which can be indexed to rhombohedral phased NiO (JCPDS No. 44–1159). Therefore, the *in situ* calcination and reduction process can be considered as two steps: nickel silicate hydrate is first decomposed into nickel oxide, and then the following reduction process converts NiO into Ni NPs.

To demonstrate the synthetic controllability, Ni/SNTs were synthesized by varying the feeding amounts of NiCl₂ under otherwise identical conditions. Fig. 6a-d shows that TEM images of NiSNTs synthesized by adding 0.1 mmol, 0.25 mmol, 0.5 mmol and 0.75 mmol NiCl₂ for hydrothermal reaction. When 0.1 mmol and 0.25 mmol NiCl₂ are added, the tube structure can be easily seen but only small amounts of petal-like units assembled on the nanotube. However, when 0.5 mmol and 0.75 mmol NiCl₂ are added, NiSNTs exhibit tubular shaped structure assembled by large amount of petal-like units. And Fig. 6e-h gives the corresponding TEM images of samples after calcination and reduction of NiSNTs. The amounts of Ni NPs on the tube are increased with the adding amounts of NiCl₂ while remaining the tube structures. Based on the ICP data (Table S1), the loading amounts of Ni can be controlled ranging from 5.6 wt. % to 23.0 wt. %. Furthermore, the BET surface area of Ni/SNTs (Table S2) is increased from 123 m²/g to 416 m²/g with the increased amount of NiCl₂.

The catalytic performance of Ni/SNTs is evaluated by catalytic reduction of 4-NP with an excess amount of NaBH₄. In Fig. 7a, upon the addition of NaBH₄, the UV-vis absorbance band immediately shift from 317 nm (assigned to 4-NP) to 400 nm (assigned to 4-nitrophenolate ion) in a typical catalytic reaction. The corresponding color changes from light yellow to bright yellow (inset in Fig. 7a). The absorption peak centered at 295 nm is assigned to 4-AP, which is colorless after the completely reduction.³⁸ Fig. 7b gives the concentration of C (C at time t) to its initial value C₀ (C/C₀) versus reaction time for the reduction of 4-NP with and without catalysts. It is found that 4-nitrophenolate ions almost cannot be reduced in the absence of catalyst. However, after adding a small amount of catalysts, the absorbance band at 400 nm successively decrease with increasing reaction time accompanied by a great amount of bubbles generated and the colour of the solution turns to colourless gradually. Fig. 7c presents the UV-vis spectra of the 4-NP reduction over 4 mg Ni/SNTs catalyst. Notably, the complete reduction of 4-NP (the peak at 400 nm disappears) only 60 s. Along with the decrease of absorbance band at 400 nm, a new need peak at 295 nm indicates the formation of 4-AP. The reduction rate can be assumed to be independent of NaBH₄ because when the initial concentration of the NaBH₄ solution is very high, it can be considered as a constant throughout the whole reduction process. Therefore, a pseudo first-order kinetic equation can be applied to evaluate the catalytic rate, which is written as $-dC/dt = dA/dt = kCt = kAt$ or $\ln(C/C_0) = \ln(A/A_0) = -kt$,³⁹ where C is the concentration of 4-NP at time t, and k is the apparent rate constant. The $\ln(C/C_0)$ vs time plot displayed in Fig.

7d exhibits a good linear correlation with reaction time. The rate constant k is calculated to be 0.084 s⁻¹, which is markedly higher than the reported catalysts based on different kinds of supports and nanoparticles with varying morphologies and sizes.^{40–46} Additionally, the rate constant of different amount of catalysts have also been investigated. In Fig. 7e, the rate constant decreases with the reduction of the catalysts amount. When adding 2 mg and 3 mg Ni/SNTs, the respective rate constant is calculated to be 0.024 s⁻¹ and 0.062 s⁻¹. Furthermore, the stability (reusability) of Ni/SNTs is studied, as displayed in Fig. 7f. It is found that the conversion remains higher than 80% even up to 10 cycles, indicating the high stability. The good stability is probably due to the unique *in situ* decomposition and reduction method, which lead to the tight assembly of Ni NPs on SNTs support that is hard to leach with repeated magnetic separation.

However, the rate constant k is not entirely reasonable to compare different supported catalysts for the loading amount is different. Therefore, the activity parameter κ which defined as the ratio of k (the rate constant) to the loading amounts of catalysts was introduced.^{21,41} And based on the ICP data (Table S1), which suggests that the loading amounts of Ni NPs is 229.8 μg/mg, κ was calculated to be 0.091 g⁻¹ s⁻¹. Table 2 gives the comparison of catalytic activities in our work and other previously reports. It can be easily found that the catalytic activity of Ni/SNTs is much higher than other supported Ni catalysts and higher than many

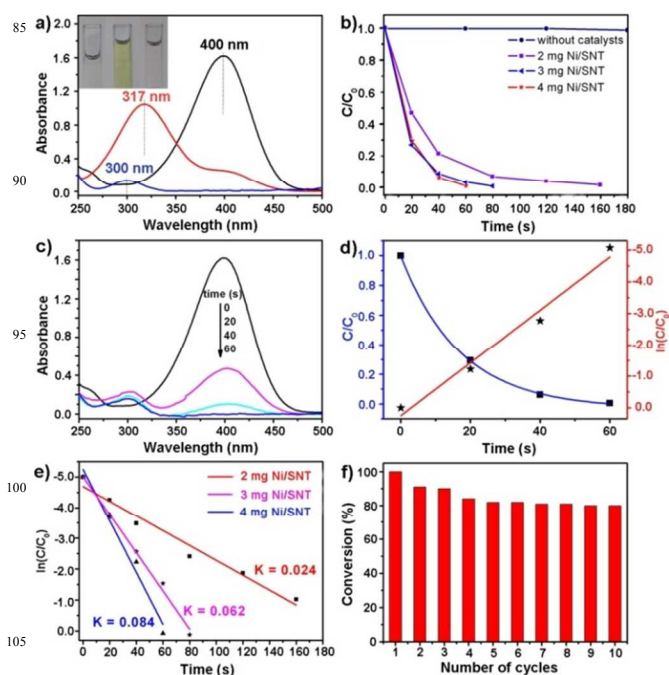


Fig. 7 a) UV-vis absorption spectra of 4-NP, 4-nitrophenolate, and 4-AP; b) C/C₀ versus reaction time for the reduction of 4-NP at the peak position of 4-NP (400 nm) using bare solution (black line), 2 mg Ni/SNTs (purple line), 3 mg Ni/SNTs (blue line) 4 mg Ni/SNTs (red line) as catalysts; c) UV-vis spectra of the catalytic reduction of 4-NP to 4-AP developed at different reaction times; d) C/C₀ and ln(C/C₀) versus time for the reduction of 4-NP over 4 mg Ni/SNTs catalysts, the ratio of 4-NP concentration (C_t at time t) to its initial value C₀ is directly represented by the relative intensity of the respective absorption peak at 400 nm; e) plot of ln(C/C₀) against the reaction time of 4-NP reduction over 2 mg Ni/SNTs (red line), 3 mg Ni/SNTs (pink line), 4 mg Ni/SNTs (blue line); f) the reusability of Ni/SNTs catalyst.

Table 2 Comparison of the activity parameter κ of composite Ni catalysts and noble catalysts for the reduction of 4-NP

Samples	Type	Supports surface	k ($\times 10^{-3} \text{ s}^{-1}$)	κ ($\times 10^{-3} \text{ mg}^{-1} \text{ s}^{-1}$)	References
Ni/SNTs (23.0 wt.%)	nanotube	hydrophilic	84	91	This work
Ni/SNTs (15.2 wt.%)	nanotube	hydrophilic	20	44	This work
Ni/SNTs (8.1 wt.%)	nanotube	hydrophilic	9.9	31	This work
Ni/SNTs (5.6 wt.%)	nanotube	hydrophilic	7.6	34	This work
Ni/CNTs	nanotube	hydrophobic	1.7	1.67	This work
Ni/SNTs (wet impregnation)	nanotube	hydrophilic	2.7	2.6	This work
RANEY® Ni	nanoparticles	N/D	0.32	0.11	27
Ni (modified)	nanoparticles	N/D	2.4	0.80	27
Ni@SiO ₂	core-shell	hydrophilic	2.8	0.94	48
Ni/p (AMPS)	Hydrogel	hydrophilic	0.9	0.15	47
RGO/Ni	nanosheet	hydrophobic	0.25	0.04	26
Fe ₃ O ₄ @SiO ₂ -Au@mSiO ₂	core-shell	hydrophilic	7	105	46
Ag-C	nanocomposite	hydrophobic	1.69	3.38	49
Au-Ag-C	nanocomposite	hydrophobic	6.46	8.7	49
Au-Fe ₃ O ₄	dumbbell-like	N/D	10.5	27.6	50
Fe ₃ O ₄ -Au	nanocomposite	N/D	6.35	14.7	19

N/D: not defined.

noble metal supported catalysts. Fig. S8 presents the UV-vis spectra of the 4-NP reduction over Ni/SNTs with different loading amounts of Ni. It is found that the larger the loading amounts of Ni, the larger the rate constant is. And κ in Table 2 indicate that the catalytic activity is enhanced with the loading amounts of Ni NPs. Furthermore, Ni/SNTs (synthesized by wet impregnation) are prepared for comparison. The UV-vis spectra of the 4-NP reduction Ni/SNTs prepared by wet impregnation are displayed in Fig. S9, a and κ are calculated based on the results. It is obvious that the catalytic activity of Ni/SNTs is much higher than that of Ni/SNTs prepared by wet impregnation method. Besides the higher specific surface area, the size of Ni NPs must be taken into account for the high catalytic activity. In Fig. S10a, it is apparent that the size of Ni NPs has a wide distribution ranging from 10 nm to 100 nm. And there are lots of large Ni NPs dissociated from the SNTs because the SNTs are too small to attach them. It is obvious that an advantage of this synthetic method is that small particle size and nearly monodisperse Ni NPs could be obtained which leads to the high catalytic reaction. The catalytic mechanism for 4-nitrophenol reduction relies on electrons from the BH₄⁻ donor to the acceptor 4-NP. In aqueous medium, BH₄⁻ is adsorbed on the surface of catalyst. After electron transfer (ET) to the metal nanoparticles, the hydrogen atom formed from the hydride, and attacked 4-NP molecules to reduce it. This ET induced hydrogenation of 4-NP occurs spontaneously.⁵¹ Therefore, hydrophilic supports surface may be easier to adsorb BH₄⁻ on the surface of Ni in the aqueous medium than hydrophobic supports. And Ni/CNTs were prepared to confirm it. The activity parameter κ was calculated to be $1.67 \times 10^{-3} \text{ mg}^{-1} \text{ s}^{-1}$ which is much slower than $91 \times 10^{-3} \text{ mg}^{-1} \text{ s}^{-1}$. We suppose that the low catalytic activity of CNTs is not only due to the low specific surface area, but also the hydrophobic nature of CNTs. Table 2 suggests that the catalytic activity of SiO₂ supported metal catalysts is higher than carbon or RGO supported catalysts. So it is possible that the hydrophilic surface of SNTs accelerate the catalytic reaction because they can easily adsorb BH₄⁻ donor on the surface of Ni NPs.

Above all, the super high catalytic rate can be due to the following factors: 1) Small particle size induced nearly monodisperse Ni NPs, which provide larger reaction area and more active sites for reduction. 2) SNTs support with large

surface area, which can load large amount of Ni NPs providing more catalytic sites and thus leading to the super catalytic activity. 3) Hydrophilic surface of SNTs which can accelerate the catalytic reaction because they easily adsorb BH₄⁻ donor on the surface of Ni NPs. 4) Ni NPs are both inside and outside of the SNTs supports, which make it convenient for catalyzing, because this kind of structure make the reactant easier to get close to the active sites.

4. Conclusions

In summary, we developed a novel and rational strategy to prepare magnetic Ni/SNTs catalysts using an *in situ* decomposition and reduction of inorganic salt precursor. The as-prepared catalyst has high specific surface area and ultra small Ni NPs size (about 6 nm) with good dispersion. The sample exhibits excellent catalytic performance in the 4-NP reduction (complete reduction of 4-NP within 60 s at room temperature). Compared with noble (Au, Pt, and Pd) catalysts grafted on various supports, the Ni/SNTs catalyst exhibits several advantages: high catalytic performance, easy for reuse and markedly lower cost. In particular, the synthetic strategy provides a useful idea for controllable synthesis other metal NPs supported nanotubes with requisite loading capacity, which should be highly potential in diverse catalytic reactions.

Acknowledgements

Financial supports from the National Natural Science Foundation of China (NSFC 21271053), Research Fund for the Doctoral Program of Higher Education of China (20112304110021), Natural Science Foundation of Heilongjiang Province (LC2012C10), Harbin Sci.-Tech. Innovation Foundation (RC2012XK017012), and the Fundamental Research Funds for the Central Universities of China are greatly acknowledged.

Notes and references

- ⁷⁵ a College of Material Science and Chemical Engineering, Harbin Engineering University, Harbin 150001, P. R. China. E-mail: yangpiaoping@hrbeu.edu.cn
 b Department of Applied Chemistry, School of Sciences, Xi'an Jiaotong University, Xi'an, 710049, P. R. China. E-mail: dingsj@mail.xjtu.edu.cn

- † Electronic supplementary information (ESI) available: XRD pattern and TEM image of SNTs after calcination, XRD pattern and EDS of NiSNTs, SEM images of a single SNT, NiSNTs and Ni/SNTs, enlarged HRTEM of Ni/SNTs, XRD pattern of NiO/SNTs, UV-vis spectra of the catalytic reduction of 4-NP to 4-AP over Ni/SNTs with different loading amounts, Ni/SNTs synthesized by wet impregnation and Ni/CNTs, TEM images of Ni/SNTs synthesized by wet impregnation and Ni/CNTs. See DOI: 10.1039/b000000x
- 1 S. Iijima, *nature* 1991, **354**, 56
 - 2 C. R. Martin and P. Kohli, *Nat. Rev. Drug Discovery* 2003, **2**, 29.
 - 3 B. C. Satishkumar, S. K. Doorn, G. A. Baker and A. M. Dattellbaum, *ACS Nano* 2008, **2**, 2283.
 - 4 K. Varghese, D. Gong, M. Paulose, K. G. Ong, E. C. Dickey and C. A. Grimes, *Adv. Mater.* 2003, **15**, 624.
 - 5 D. T. Mitchell, S. B. Lee, L. c. m. Trofin, N. Li, T. K. Nevanen, H. Söderlund and C. R. Martin, *J. Am. Chem. Soc.* 2002, **124**, 11864.
 - 6 X. L. Pan and X. H. Bao, *Chem. Comm.* 2008, **47**, 6271.
 - 7 H. Q. Li, L. N. Han, J. White and Kim, *Green Chem.* 2012, **14**, 586.
 - 8 C. C. Chen, Y. C. Liu, C. H. Wu, C. C. Yeh, M. T. Su and Y. C. Wu, *Adv. Mater.* 2005, **17**, 404.
 - 9 J. H. Park, S. Kim and A. J. Bard, *Nano Lett.* 2006, **6**, 24.
 - 10 Z. Chen, J. Appenzeller, J. Knoch, Y.-m. Lin and P. Avouris, *Nano Lett.* 2005, **5**, 1497.
 - 11 H. Q. Cao, L. D. Wang, Y. Qiu, Q. Z. Wu, G. Z. Wang, L. Zhang and X. W. Liu, *Chemphyschem* 2006, **7**, 1500.
 - 12 M. A. Zeeshan, S. Pane, S. K. Youn, E. Pellicer, S. Schuerle, J. Sort, S. Fusco, A. M. Lindo, H. G. Park and B. J. Nelson, *Adv. Funct. Mater.* 2013, **23**, 823.
 - 13 F. F. Tao, M. Y. Guan, Y. Jiang, J. M. Zhu, Z. Xu and Z. L. Xue, *Adv. Mater.* 2006, **18**, 2161.
 - 14 X. L. Yu, C. B. Cao and X. Q. An, *Chem. Mater.* 2008, **20**, 1936.
 - 15 K. Nielsch, F. J. Castañó, S. Matthias, W. Lee and C. A. Ross, *Adv. Eng. Mater.* 2005, **7**, 217.
 - 16 W. Lee, R. Scholz, K. Nielsch and U. Gösele, *Angew. Chem. Int. Ed.* 2005, **44**, 6050.
 - 17 S. K. Hashmi and G. J. Hutchings, *Angew. Chem. Int. Ed.* 2006, **45**, 7896.
 - 18 V. Rode, M. J. Vaidya and R. V. Chaudhari, *Org. Process. Res. Dev.* 1999, **3**, 465.
 - 19 Y. C. Chang and D. H. Chen, *J. Hazard. Mater.* 2009, **165**, 664.
 - 20 Wang, X. B. Zhang, Z. L. Wang, L. M. Wang, W. Xing and X. Liu, *Nanoscale* 2012, **4**, 1549.
 - 21 B. Baruah, G. J. Gabriel and M. J. Akbashev, M. E. Booher, *Langmuir* 2013, **29**, 4225.
 - 22 S. C. Tang, S. Vongehr and X. K. Meng, *J. Mater. Chem.* 2010, **20**, 5436.
 - 23 A. Gangula, R. Podila, M. Ramakrishna, L. Karanam, C. Janardhana and A. M. Rao, *Langmuir* 2011, **27**, 15268.
 - 24 S. Zhou, K. McIlwrath, G. Jackson and B. Eichhorn, *J. Am. Chem. Soc.* 2006, **128**, 1780.
 - 25 S. Senapati, S. K. Srivastava, S. B. Singh and H. N. Mishra, *J. Mater. Chem.* 2012, **22**, 6899.
 - 26 Z. Ji, X. Shen, G. Zhu, H. Zhou and A. Yuan, *J. Mater. Chem.* 2012, **22**, 3471.
 - 27 Z. Jiang, J. Xie, D. Jiang, X. Wei and M. Chen, *Crystengcomm* 2013, **15**, 560.
 - 28 L. Zhou, C. Gao and W. Xu, *Langmuir* 2010, **26**, 11217.
 - 29 Y. Zhu, J. Shen, K. Zhou, C. Chen, X. Yang and C. Li, *J. Phys. Chem. C* 2011, **115**, 1614.
 - 30 Z. Zhang, C. Shao, P. Zou, P. Zhang, M. Zhang, J. Mu, Z. Guo, X. Li, C. Wang, Y. Liu, *Chem. Commun.* 2011, **47**, 3906.
 - 31 J. Lee, J. C. Park and H. Song, *Adv. Mater.* 2008, **20**, 1523.
 - 32 K. Jiang, H.-X. Zhang, Y.-Y. Yang, R. Mothes, H. Lang and W.-B. Cai, *Chem. Commun.* 2011, **47**, 11924.
 - 33 Y. Wang, G. Wang, H. Wang, C. Liang, W. Cai and L. Zhang, *Chem. Eur. J.* 2010, **16**, 3497.
 - 34 J. Qu, W. Li, C.-Y. Cao, X.-J. Yin, L. Zhao, J. Bai, Z. Qin and W.-G. Song, *J. Mater. Chem.* 2012, **22**, 17222.
 - 35 Y. Lee, J. Lee, C. J. Bae, J. G. Park, H. J. Noh, J. H. Park and T. Hyeon, *Adv. Funct. Mater.* 2005, **15**, 503.
 - 36 D. Chen, J. Li, C. Shi, X. Du, N. Zhao, J. Sheng and S. Liu, *Chem. Mater.* 2007, **19**, 3399.
 - 37 J. Liu, G. Qin, P. Raveendran and Y. Ikushima, *Chem. Eur. J.* 2006, **12**, 2131.
 - 38 R. Xu, T. Xie, Y. Zhao and Y. Li, *Nanotechnology* 2007, **18**.
 - 39 M. Schrunner, M. Ballauff, Y. Talmon, Y. Kauffmann, J. Thun, M. Möller and J. Breu, *Science* 2009, **323**, 617.
 - 40 R. Liu, S. M. Mahurin, C. Li, R. R. Unocic, J. C. Idrobo, H. Gao, S. J. Pennycook and S. Dai, *Angew. Chem. Int. Ed.* 2011, **50**, 6799.
 - 41 Q. An, M. Yu, Y. Zhang, W. Ma, J. Guo, C. and Wang, *J. Phys. Chem. C* 2012, **116**, 22432.
 - 42 J. Li, C.-y. Liu and Y. Liu, *J. Mater. Chem.* 2012, **22**, 8426.
 - 43 X. Wang, Y. Cui, Y. Wang, X. Song and J. Yu, *Inorg. Chem.* 2013, **52**, 10708.
 - 44 J. Liu, G. Qin, P. Raveendran and Y. Ikushima, *Chem. Eur. J.* 2006, **12**, 2131.
 - 45 H. Li, J. K. Jo, L. Zhang, C.-S. Ha, H. Suh and I. Kim, *Adv. Funct. Mater.* 2010, **20**, 3864.
 - 46 Y. H. Deng, Y. Cai, Z. K. Sun, J. Liu, C. Liu, J. Wei, W. Li, C. Liu, Y. Wang and D. Y. Zhao, *J. Am. Chem. Soc.* 2010, **132**, 8466.
 - 47 N. Sahiner, H. Ozay, O. Ozay and N. Aktas, *Appl. Catal. A-Gen.*, 2010, **385**, 201.
 - 48 Z. Jiang, J. Xie, D. Jiang, J. Jing and H. Qin, *CrystEngComm*, 2012, **14**, 4601.
 - 49 B. Guan, X. Wang, Y. Xiao, Y. Liu and Q. Huo, *Nanoscale*, 2013, **5**, 2469.
 - 50 F.-H. Lin and R.-A. Doong, *J. Phys. Chem. C*, 2011, **115**, 6591.
 - 51 J.-P. Deng, W.-C. Shih and C.-Y. Mou, *J. Phys. Chem. C*, 2007, **111**, 9723.